Supporting Information

Efficient and Scalable High-Quality Graphene Nanodot Fabrication through Confined Lattice Plane Electrochemical Exfoliation

Hui Wang,‡[a] Kaiyi Zhu,‡[a] Liwei Yan,[a] Can Wei,[a] Yu Zhang,[b] Chunhong Gong,[b] Jianhui Guo,[a] Jiwei Zhang,[a] Dongmao Zhang*[c,d] and Jingwei Zhang*[a,e]

[a] National & Local Joint Engineering Research Center for Applied Technology of Hybrid Nanomaterials, Henan University, Kaifeng, China.

[b] College of Chemistry and Chemical Engineering, Henan University, Kaifeng, China.

[c] Department of Chemistry, Mississippi State University, Starkville, MS, United States.

[d] Department of Chemistry, Xihua University, Chengdu, China.

[e] Collaborative Innovation Center of Nano Functional Materials and Applications of Henan Province, Henan University, Kaifeng, China.

Corresponding Author E-mail address:

jwzhang@henu.edu.cn (J.W. Zhang); dongmao@chemistry.msstate.edu (D.M. Zhang)

Content   Page No.

S1. Experimental details for GNDs synthesis method and characterization.

EXPERIMENTAL

Materials

Highly oriented pyrolytic graphite (HOPG) was purchased from Beijing Great Wall Co., Ltd (Beijing, China, 0.8 ± 0.2º FWHM (refers to full width half maximum) grade B). Analytical grade NaOH (analytical reagent, AR) was bought from Tianjin Kermel Chemical Reagent Co., Ltd (Tianjin, China). Paraffin wax was purchased from Shanghai Specimen and Model Factory (Shanghai, China).

GNDs preparation

Fig. S1 illustrates the confined lattice plane electrochemical exfoliation experiment setup for GND preparation. Briefly, the HOPG (size, 1 cm × 1 cm × 0.05 cm) as the working electrode was covered by paraffin while either its bottom or side was exposed to 10 M NaOH. The counter electrode (a nickel foam) was placed 1.0 cm away from the working electrode. A direct current (dc) power supply is used to offer the voltage (about 4 V) to the electrodes at room temperature. Unless specified otherwise, all the exfoliation processes was carried out for 5 hrs. The GND aqueous solution (a stable and neutral (pH=7) homogeneous brownish yellow solution) was obtained by dialysis of the diluted electrolyte after electrolysis reaction in deionized water (a dialysis bag with the retain molecular weight 3500 Da was used) for 3 days. All dialyzed products from the two FER and SER processes are permeable through the filtration membrane that used for separating GNDs from large graphene particles. The pore size of the filtration membrane is 220 nm (Shanghai Xingya Purifying Materials Factory, China).

Hydrothermal treatment of the GND was performed by keeping the GND aqueous solution in a pressurized reactor (50 mL poly(tetrafluoroethylene)(Teflon)-lined autoclave) at 200 ºC for 24 hrs. The fluorescence activity of the treated samples is then compared with the as-obtained GNDs.

Characterizations

The morphology of the fGNDs, sGNDs, wGNDs and fGQDs were analyzed with a transmission electron microscope (TEM, JEM-2100F, JEOL Ltd., Japan). The thickness of the fGNDs, sGNDs, wGNDs and graphene sheets were analyzed with an atomic force microscope (AFM, Bruker Nano Inc., Dimension Icon, USA). The AFM images were captured at ambient conditions in tapping mode (resolution, Z < 0.3 Å, XY < 0.2 nm) with the samples deposited on freshly cleaved mica substrates. Significantly reduced noise floor enables imaging at atomic level in contact mode with less than 0.03 nm in Tapping Mode. All images were captured in the standard tapping mode in order to minimize force acting on the GNDs layer, while the scan rate was 0.977 Hz. The captured images were processed afterwards in the NanoScopeAnalysis software by 1st order flattening. Then click on the section option of the software and pull out a height line on the image, at this time, the software automatically deducts the height of substrates and obtains the true thickness profile of the samples.

The surface chemical component of the fGNDs and fGQDs were analyzed with an Escalab 250Xi X-ray photoelectron spectroscopy (XPS, Thermo Fisher Scientific, USA). The ultraviolet-visible light (UV-vis) spectra of the as-prepared GNDs aqueous

solution were measured with an UV-2600 spectrophotometer (Shimadzu, Japan). O_3 detection was conducted with ozone test strips purchased from Macherey-Nagel (Germany). The morphology and structure of FER anode were analyzed with a scanning electron microscope (Nova Nano SEM 450, FEI, USA). Raman measurements were conducted with a Renishaw in Via Raman spectrometer (Renishaw inVia, Renishaw, UK) under the laser excitation at 532 nm with the GNDs were put on Si substrate. The experimental conditions of Raman measurements are as follows: the total laser energy is 500 mW, the power on sample is 10% (50 mW) of the total laser energy. The range of Raman shift is 600-3000 cm^{-1} and the resolution is 0.5 cm^{-1}. Furthermore, all Raman spectra were treated by origin Pro 8.5 software to fit peaks. All spectra can be resolved into D peak and G peak. Lorentz fitting was used to determine the integral intensities of D peak and G peak. I_D/I_G was the corresponding ratio of D peak integral intensity to G peak integral intensity. In fGNDs Raman spectra, D peak integral intensity was 207168, G peak integral intensity was 201134, I_D/I_G =1.03. In sGNDs Raman spectra, D peak integral intensity was 134051, G peak integral intensity was 141107, I_D/I_G =0.95. In wGNDs Raman spectra, D peak integral intensity was 232683, G peak integral intensity was 258537, I_D/I_G =0.90.

Fluorescent emission-excitation spectra and the absolute fluorescence quantum yield (QY) were recorded with a JY HORIBA FluoroLog-3 spectrofluorometer (JY Horiba Inc. France), while the model of the integration sphere used in spectrofluorometer is Quanta-φ. First, GNDs aqueous solution diluted to the absorbance of 0.04 at 340 nm wavelength was prepared for absolute fluorescence

quantum yield test, GQDs aqueous solution diluted to the absorbance of 0.04 at 310

nm wavelength was prepared for absolute QY test, because 340 nm is the optimal

excitation wavelength of GNDs and 310 nm is the optimal excitation wavelength of

GQDs. Second, turn on the absolute QY measurement mode of the JY HORIBA

FluoroLog-3 spectrofluorometer with the Quanta-φ model of the integration sphere

used in spectrofluorometer. Thirdly, before determining the absolute QY of the

samples, the effect of solvent-deionized water substrates is deducted by the JY

HORIBA FluoroLog-3 spectrofluorometer, and then the absolute QY of the sample is

tested at the optimal excitation wavelength. The absolute QY is calculated by the

following expression,

The absolute QY= number of emitted photons / number of absorbed photons

$$\text{The absolute QY}_{\text{fGNDs}} \text{ at 340 nm excitation} = \int_{360}^{660} \frac{E_{\text{fGNDs}} - E_{H_2O}}{A_{\text{fGNDs}} - A_{H_2O}}$$

$$\text{The absolute QY}_{\text{fGQDs}} \text{ at 310 nm excitation} = \int_{330}^{600} \frac{E_{\text{fGQDs}} - E_{H_2O}}{A_{\text{fGQDs}} - A_{H_2O}}$$

E_{fGNDs} is the emission intensity of fGNDs, E_{H2O} is the emission intensity of H_2O,

A_{fGNDs} is the absorption intensity of fGNDs, A_{H2O} is the absorption intensity of H_2O,

360-660 is the wavelength range of emission fluorescence spectrum of fGNDs. E_{fGQDs}

is the emission intensity of fGQDs, E_{H2O} is the emission intensity of H_2O, A_{fGQDs} is

the absorption intensity of fGQDs, A_{H2O} is the absorption intensity of H_2O, 330-600 is

the wavelength range of emission fluorescence spectrum of fGQDs.

Finally, the absolute QY is calculated automatically and provided by the JY HORIBA FluoroLog-3 spectrofluorometer with the Quanta-φ model of the integration sphere used in spectrofluorometer.

S2. Schematics of experimental set-up and the anodes used FER, SER, and WER processes.
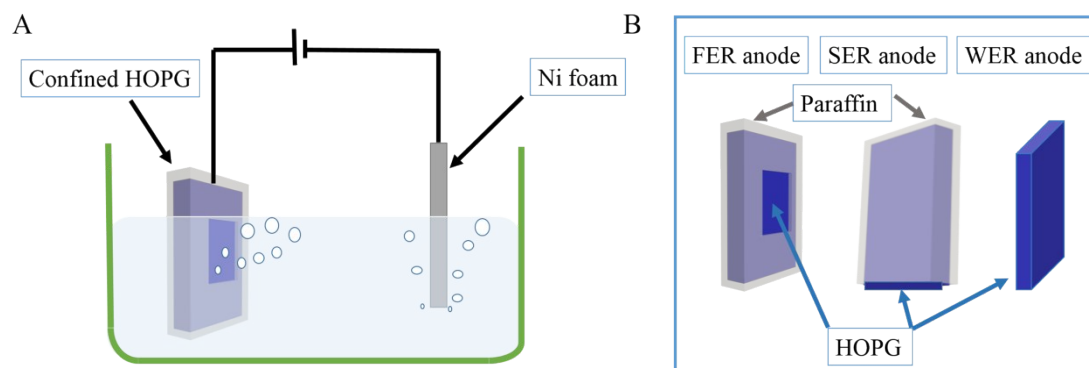

Fig. S1 (A) Schematics of the confined lattice plane electrochemical exfoliation process. (B) Schematic representation of the crystal planes exposed in the FER, SER and WER process. The areas exposed during the FER, SER, and WER processes are shown in blue. The areas in gray are covered with paraffin.

S3. Photographs of the anodes used in FER, SER, and WER before and after electrolysis.
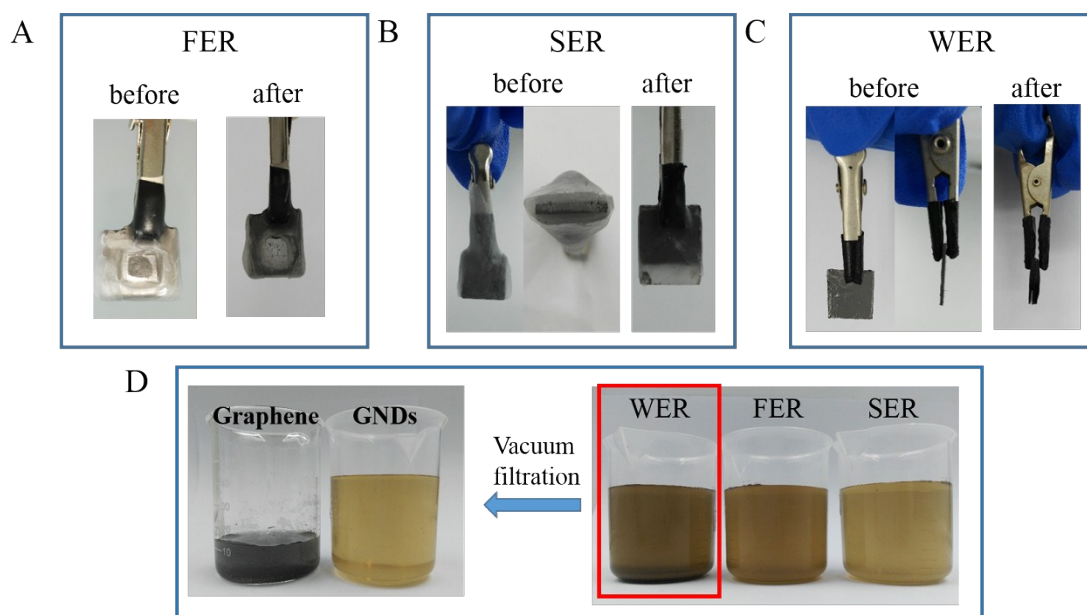

Fig. S2 Photographs of the anodes used in (A) FER, (B) SER and (C) WER before and after electrolysis. (D) The products obtained with the FER, SER and WER processes. The photograph of container labeled as "graphene" is obtained by redispersing the materials retaining on the filtration membrane with a pore size of 0.2 µm. There is no significant material retaining on the membrane when the products from the FER or SER processes is vacuum filtered.

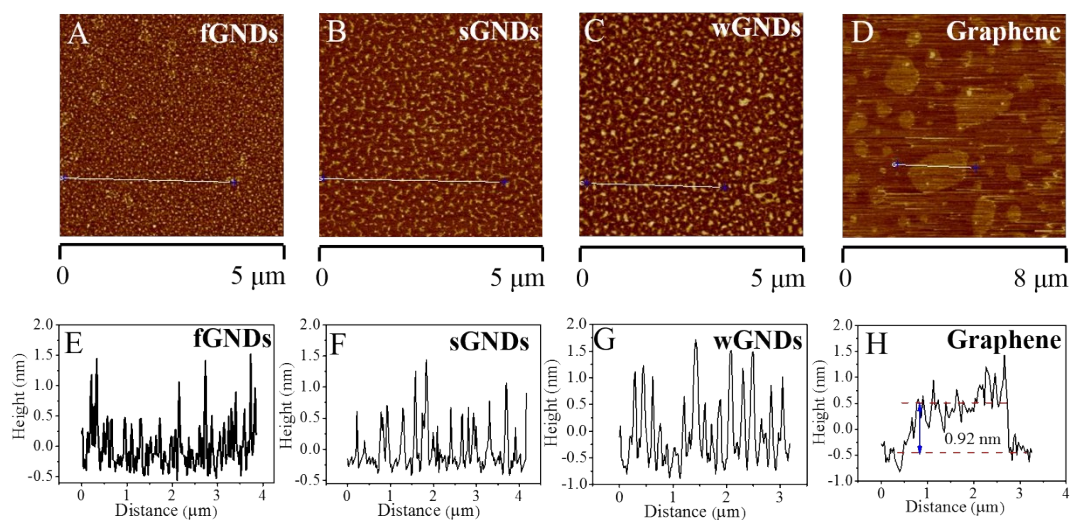**S4. AFM images and thickness analysis of fGNDs, sGNDs, wGNDs.**

Fig. S3 (Top) AFM images and (Bottom) corresponding thickness profile along the line (inset) of (A, E) fGNDs, (B, F) sGNDs, (C, G) wGNDs, respectively. (D) and (H) are the AFM image of graphene nanosheets obtained with WER process and its corresponding thickness profile, respectively. (E, F, G, H) are the true height profiles of the samples, because the NanoScopeAnalysis software automatically deducts the height of substrates.

S5. Ozone strip testing of the ozone generation during the WER, SER, and FER process, XPS spectra and Raman spectra of fGNDs, sGNDs, wGNDs.
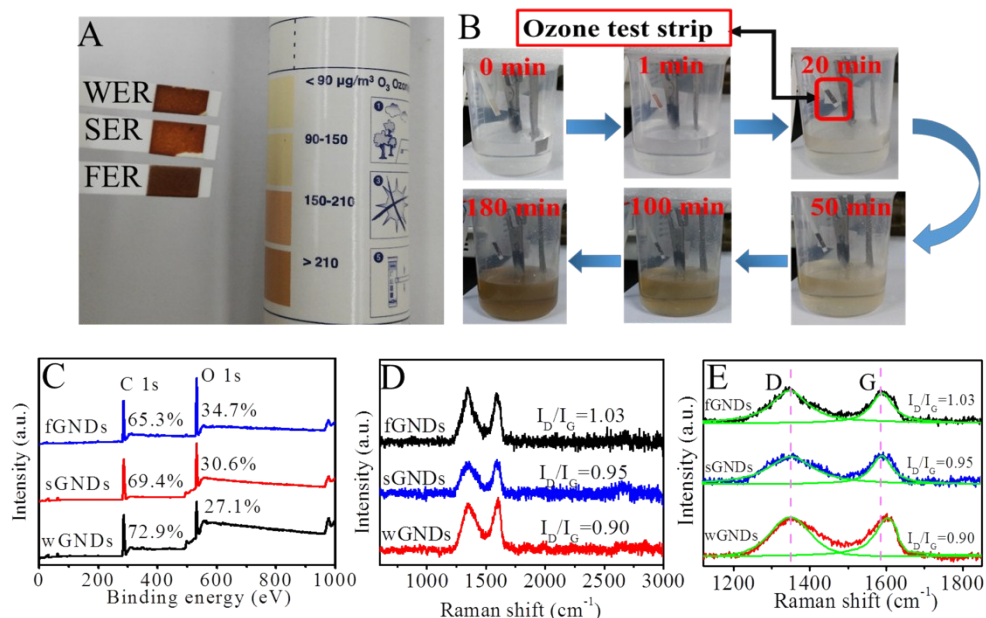

Fig. S4 (A) ozone strip testing of the ozone generation during the WER, SER, and FER process in 10 M NaOH. The reaction conditions are the same (electrolysis voltage 4 V, electrode distance 1 cm, testing time 3 min). (B) The color change of ozone test strip and electrolyte solution at different stages of FER. (C) XPS spectra of (black) wGNDs, (red) sGNDs, and (blue) fGNDs. (D, E) Raman spectra of (red) wGNDs, (blue) sGNDs, and (black) fGNDs. In Fig. S4 (E), the Raman spectra was resolved into D and G bands, as indicated by green lines.

S6. Performance comparison of the GQDs fabricated with the FER method and that prepared with literature top-down methods.

Table S1. Comparison of conversation yield, fluorescence quantum yield, and particle size of GQDs prepared with top-down methods that use carbon-based starting materials.

Materials	Method	Yield/ %	QY/ %	Size/ nm	Byproducts	Separation	Ref.
Graphene oxide	Hydrothermal treatment	22	6.9	2-16	Large graphene oxide nanoparticles	Filtration	[1]
Fullerene	metal-catalysedcage-opening of $C_{60.}$	67	~	0.6-1.6	Carbon clusters	~	[2]
Hexa-peri-hexabenzo coronene	Carbonization + modified Hummers method	~	3.8	~60	~	~	[3]
Graphene oxide	Microwave-assisted acid oxidation	33	22.9	2-7	Large particles graphene oxide	Filtration	[4]
Carbon Fibers	Acidic oxidation and cutting	~	~	1-4	No byproducts	Without separation	[5]
3D graphene	Electrochemically exfoliation	~	10	1-5	Large graphene particles	Centrifugation	[6]
Graphite	microwave irradiation+ oxidation	70	9	2–10	large graphene nanoparticles	Filtration	[7]
Graphene oxide	Hydrothermal treatment	~	~	2.5-6	large graphene nanoparticles	Filtration	[8]
Graphite	Micro fluidization	0.3	1.32	1-5	Large graphene particles	Filtration	[9]
Graphite	Ultrasound-induced liquid-phase exfoliation	0.9	4.7	10-25	Unexfoliated graphitic	Centrifugation	[10]
Graphite	Solvothermal method	10	8.8	1-5	No byproducts	Without separation	[11]
HOPG	FER	89	31.1	1-5 nm	No byproducts	Without separation	This work

S7. XPS analysis of carbon species in fGNDs and fGQDs.

Table S2. XPS analysis of carbon species in fGNDs and fGQDs.

Sample	C-C (%)	C-O (%)	C=O (%)	O-C=O (%)	QY (%)	optimal excitation wavelength / nm	maximum emission wavelength / nm	FWHM/ nm
fGNDs	44.2	42.1	8.1	8.6	4.1	340	445	82
fGQDs	39.2	50.4	3.7	6.7	31.1	310	375	75

S8. Comparison of fluorescence quantum yield of fGNDs vs fGQDs, sGNDs vs. sGQDs, and wGNDs vs. wGQDs.

Table S3. A head-to-head comparison of fluorescence quantum yield of fGNDs vs fGQDs, sGNDs vs. sGQDs, and wGNDs vs. wGQDs.

Sample	QY (%)
fGNDs/ fGQDs	4.1/31
sGNDs/sGQDs	3.5/17
wGNDs/ wGQDs	3.2/15

REFERENCES

1 D. Pan, J. Zhang, Z. Li and M. Wu, *Adv. Mater.*, 2010, **22**, 734-738.

2 L. Jiong, Y. P. Shan Emmeline, G. Chee Kwan, W. Ping and L. Kian Ping, *Nat. Nanotechnol.*, 2011, **6**, 247−252.

3 L. Ruili, W. Dongqing, F. Xinliang and M. Klaus, *J. Am. Chem. Soc.*, 2011, **133**, 15221-15223.

4 L. L. Li, J. Ji, R. Fei, C. Z. Wang, Q. Lu, J. R. Zhang, L. P. Jiang and J. J. Zhu, *Adv. Funct. Mater.*, 2012, **22**, 2971-2979.

5 J. Peng, W. Gao, B. K. Gupta, Z. Liu, R. Romeroaburto, L. Ge, L. Song, L. B. Alemany, X. Zhan and G. Gao, *Nano Lett.*, 2012, **12**, 844-849.

6 A. Ananthanarayanan, X. Wang, P. Routh, B. Sana, S. Lim, D. H. Kim, K. H. Lim, J. Li and C. Peng, *Adv. Funct. Mater.*, 2014, **24**, 3021-3026.

7 Y. Shin, J. Lee, J. Yang, J. Park, K. Lee, S. Kim, Y. Park and H. Lee, *Small*, 2014, **10**, 866-870.

8 Q. Zhang, J. Jie, S. Diao, Z. Shao, Q. Zhang, L. Wang, W. Deng, W. Hu, H. Xia and X. Yuan, *ACS Nano*, 2015, **9**, 1561-1570.

9 M. Buzaglo, M. Shtein and O. Regev, *Chem. Mater.*, 2016, **28**, 21-24.

10 A. Ciesielski, S. Haar, A. Aliprandi, M. E. Garah, G. Tregnago, G. F. Cotella, M. E. Gemayel, F. Richard, H. Sun and F. Cacialli, *ACS Nano*, 2016, **10**, 10768−10777.

11 B. Liu, J. Xie, H. Ma, X. Zhang, Y. Pan, J. Lv, H. Ge, N. Ren, H. Su and X. Xie, *Small*, 2017, **13**, 1601001.